Research Article | Vol. 10, No. 1 / 1 January 2020 / Optical Materials Express 46
Optical Materials EXPRESS

MoS_2/graphene heterostructure incorporated passively mode-locked fiber laser: from anomalous to normal average dispersion

HUANHUAN LIU, ZILONG LI, WEI SONG, YE YU, FUFEI PANG,* AND TINGYUN WANG

Key Laboratory of Specialty Fiber Optics and Optical Access Networks, Joint International Research Laboratory of Specialty Fiber Optics and Advanced Communication, Shanghai Institute for Advanced Communication and Data Science, Shanghai University, 99 Shangda Road, Shanghai, 200444, China
*ffpang@shu.edu.cn

Abstract: Two-dimensional (2D) nanomaterials for ultrafast photonic applications have attracted significant attention in recent years. 2D nanocomposites are of great interest because of their capability to combine the merits of each nanomaterial. In this work, we have demonstrated erbium-doped mode-locked fiber lasers that incorporate MoS_2/graphene heterostructure based saturable absorbers (SAs) from anomalous to normal average dispersion for the first time. The modulation depth, the saturation intensity, and the non-saturable absorption of the MoS_2/graphene heterostructure are measured to be 12.4%, 12.7 MW/cm^2 and 28%, respectively. By incorporating this particular MoS_2/graphene heterostructure based SA, the mode-locked fiber lasers can produce stable pulse trains at anomalous, near-zero, and normal average dispersion. At an anomalous average dispersion of -0.181 ps^2, the Kelly sidebands are found to be superimposed on the optical spectrum, and a stable soliton pulse train has been measured with a signal-to-noise ratio of ~73 dB in the radio frequency spectrum. At a near-zero average dispersion of -0.082 ps^2, a Gaussian-like optical spectrum has been observed where the narrowest pulse width is ~837 fs. At normal average dispersion of + 0.041 ps^2, the steep-edge optical spectrum has been produced, indicating that dissipative solitons have been generated. The obtained results prove that a MoS_2/graphene heterostructure is an ideal SA in mode-locked fiber lasers for ultrashort pulse generation from anomalous to normal average dispersion.

1. Introduction

Ultrashort pulse has attracted much attention because of its wide application in scientific and industrial fields including optical communication, optical sensing, micromachining, supercontinuum generation, laser surgery, biological medicine, *etc* [1–6]. In particular, the passively mode-locked fiber lasers that generate ultrashort pulse have developed rapidly [7–10] due to good beam quality, flexibility, robustness, compactness, low cost, *etc* [11–14]. In order to control the pulse width, the dispersion-managed fiber lasers are of great interest [15,16]. By adjusting the average dispersion of the laser cavity, the output of fiber laser could generate different types of pulses. At anomalous average dispersion, the mode-locked fiber laser can generate the traditional solitons with chirp-free feature [17]. When the net average dispersion is near-zero, dispersion-management solitons with largest spectral bandwidth as well as narrowest pulse width can be obtained [18]. At normal average dispersion region, in addition to satisfy the balance between nonlinearity and dispersion, the dissipative solitons must reach the balance between loss and gain, and thus the dissipative solitons are highly chirped with large pulse energy [19,20].

One of the key components for achieving passive mode-locking in fiber lasers is saturable absorber (SA). In addition to the artificial SAs such as nonlinear polarization rotation (NPR) method [21], the two-dimensional (2D) nano-materials have explored recently for being SAs

#381967 https://doi.org/10.1364/OME.10.000046
Journal © 2020 Received 1 Nov 2019; revised 22 Nov 2019; accepted 22 Nov 2019; published 2 Dec 2019

Optical Materials EXPRESS

including graphene [22–25], graphene oxide [26], black phosphorus [27–29], transition-metal dichalcogenides like Molybdenum disulfide (MoS_2) [30–34], topological insulator (TI) [35] and other 2D materials [36–44]. Especially, graphene has attracted for being SAs owing to its ultrafast dynamic response, wavelength-independent saturable absorption, extremely high carrier mobility and good material flexibility [22,45]. On one hand, zero bandgap of graphene is benefit for broadband SAs. On the other hand, the monolayer graphene has relative weak absorption and thus low modulation depth [46]. MoS_2 has large bandgap (1 eV for bulk and 2 eV for monolayer) [47], showing it an ideal candidate for optoelectronic devices. However, its intraband relaxation time is longer than that of graphene, and monolayer MoS_2 is easily oxidized under high-energy laser irradiation [48], which restricting its ability to adjust ultrashort laser pulse.

In addition to explore individual 2D nanomaterials, heterostructures, which have been synthesized by stacking at least two materials with different band structure, have attracted much attention due to their unique physical, chemical, structural properties and potential application in optoelectronic devices [48–51]. Compared with individual 2D devices, van der Waals heterostructure devices provide abundant opportunities in both basic researches and device applications due to their remarkable versatility and advantages in functions and performance [52]. By comparing graphene with MoS_2, it is possible to complement each other: the zero bandgap and low optical absorption of graphene can be complemented by MoS_2 [53,54]. Compared with graphene and MoS_2 for ultrafast photonics, the MoS_2/graphene nanocomposites possess equivalent saturable intensity along with larger modulation depth [55]. He *et al* have demonstrated that the modulation depth and saturation intensity of MoS_2/Graphene nanocomposite films are material thickness depended [56]. However, the application of MoS_2/graphene heterostructure in dispersion-managed mode-locked fiber laser has not yet been reported.

In this work, the dispersion-managed mode-locked fiber lasers from anomalous to normal average dispersion incorporating with MoS_2/grapheneheterostructure based SA have been demonstrated for the first time. The MoS_2/grapheneheterostructure based SA shows the modulation depth, the saturation intensity and the non-saturable absorption of 12.4%, 12.7 MW/cm^2 and 28%, respectively. When the mode-locked fiber laser operates at average anomalous dispersion of -0.181 ps^2, the traditional solitons with the Kelly sidebands are produced showing signal-to-noise ratio of ~73 dB. By managing the cavity average dispersion to be -0.082 ps^2, a Gaussian-like optical spectrum has been observed where the narrowest pulse-width can be achieved to be ~837 fs. At normal average dispersion of + 0.041 ps^2, the dissipative solitons with the steep-edge optical spectrum have been produced. The obtained results indicate that the MoS_2/graphene heterostructure based SAs have great potential in dispersion-managed mode-locked fiber laser for ultrashort pulse generation from anomalous to normal average dispersion.

2. Numerical simulation

Generally, an erbium-doped mode-locked fiber laser consists of the erbium-doped fiber (EDF), the single-mode fiber (SMF), and SA. The pulse evolution along either EDF or SMF can be modeled by the extended nonlinear Schrödinger equation as [57]**:**

$$\frac{\partial A(\xi,T)}{\partial \xi}+\frac{i}{2}\left(\beta^{(2)}+ig\frac{1}{\Omega_g^2}\right)\frac{\partial^2 A(\xi,T)}{\partial T^2}=i\gamma|A(\xi,T)|^2A(\xi,T)+\frac{g}{2}A(\xi,T) \tag{1}$$

where $A(\xi,T)$ is the slowly varying amplitude of the pulse envelope; ξ is the propagation coordinate; T is pulse duration; $\beta^{(2)}$ is the second-order dispersion parameter; γ represents the nonlinear parameter; Ω_g is the gain bandwidth; and g is the gain coefficient which is modeled by:

$$g=g_0/(1+P_{ave}/P_{sat}) \tag{2}$$

Optical Materials EXPRESS

where g_0 is the small signal gain, P_{sat} is the gain saturation power, and P_{ave} is the average power of pulses.

The transmittance of SA can be modeled by:

$$T(I) = 1 - (a_0/(1 + I/I_{sat}) + a_{ns}) \tag{3}$$

where $T(I)$ is the transmission, a_0 is the modulation depth, I is the input intensity, I_{sat} is the saturation intensity and a_{ns} is the non-saturable absorbance.

$$\beta^{(2)}_{ave} = \sum_{i=1}^{N} \beta^{(2)}_{fiber\ i} \times L_{fiber\ i} \tag{4}$$

where $\beta^{(2)}_{ave}$ is the cavity average dispersion; $\beta^{(2)}_{fiber\ i}$ is the second-order dispersion parameter of different types of fiber including EDF, HI1060 type fiber, and SMF; $L_{fiber\ i}$ is the corresponding fiber length.

Based on above equations, we have simulated the pulse generation where the parameters are listed as in Table 1. The modulation depth a_0, the saturation intensity I_{sat} and the non-saturable absorbance a_{ns} is 12.4%, 12.7 MW/cm^2 and 28%, respectively. Figure 1(a) simulates the soliton evolution against cavity round number with the anomalous average dispersion. After the pulse is amplified by the gain fiber, it experiences the periodic perturbations, for instance, filtering, gain, and loss. The dispersive wave generated from the periodic perturbations exchanges energy with the propagating soliton, which leads to the Kelly sidebands on the spectrum. Due to the balance between the intra-cavity dispersion and nonlinearity, the stable conventional solitons are obtained [15]. After 50 rounds trip, a stable optical spectrum can be obtained.

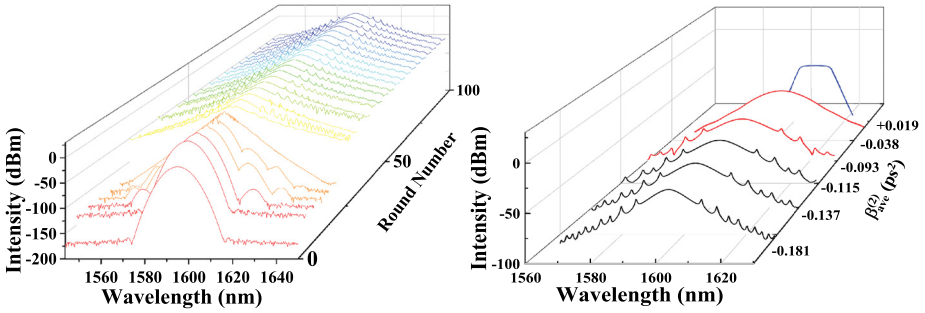

Fig. 1. (a) Pulse evolution against cavity round number; (b) soliton state of fiber laser obtained by simulation from anomalous to normal average dispersion.

Table 1. Summary of simulation parameters

Fiber Type	$\beta^{(2)}(ps^2/km)$	$\gamma(W^{-1}km^{-1})$	$L(m)$
EDF	+14.2	2.69	7.26
HI1060	-7	1.5	1.6
SMF	-22	1.09	Var.

EDF, erbium-doped fiber; SMF, single-mode fiber; Var., variable.

By varying the length of SMF, the average dispersion of the laser cavity can be managed. At anomalous cavity average dispersion range, the pulses that propagate inside the laser cavity experience the balance between the intra-cavity dispersion and nonlinearity, the conventional

Optical Materials EXPRESS

solitons can be obtained. While the cavity average dispersion nears zero, the pulses are stretched and compressed by the two opposite dispersion fibers, the dispersion-management solitons are obtained. Different from the conventional solitons, except the effect of the balance between the intra-cavity dispersion and nonlinearity, the other balance between gain and loss plays an important role in generation of the dissipative solitons while the cavity average dispersion is at normal average dispersion region [57]. As shown in Fig. 1(b), in the initial state, when the length of SMF is 12.4 m corresponding to the cavity average dispersion of -0.181 ps^2, the Kelly sidebands on the optical spectrum indicate that the fiber laser works in anomalous dispersion regime. Then, we decrease the length of SMF to increase the cavity average dispersion. When the cavity average dispersion approaches -0.038 ps^2, the dispersion-managed soliton is achieved with Kelly sidebands far from center wavelength on optical spectrum. As the cavity average dispersion increases up to + 0.019 ps^2, the steep-edge profile of optical spectrum indicates that the mode-locked fiber laser produces dissipative soliton.

3. Preparation and characterization of the MoS_2/graphene heterostructure

The materials used in our work are commercial-grade MoS_2 grown onto sapphire, and graphene grown onto copper foil, respectively. The preparation process of MoS_2/graphene heterostructure is illustrated in Fig. 2. Firstly, a water-assisted transfer process is employed to transfer the MoS_2 from sapphire onto the end-facet of a standard fiber connector [58]. The inset shows the atomic force microscopic (AFM) image of MoS_2 film. The thickness of the film is around 3.2 nm, indicating that about five layers have been explored. Simply, we use a needle to poke the MoS_2 along the edge of it gently to generate cracks. Then the sample is immersed into deionized water slowly. Due to different surface energies between MoS_2 and sapphire, MoS_2 film can float on the surface of water while the sapphire is submerged [59]. Next, we attach MoS_2 film to the end-facet of a fiber connector and dry in a vacuum drying oven. Secondly, graphene film is transferred onto the fiber connector, which is covered by MoS_2 film via wet transfer techniques [60]. Briefly, the graphene/copper foil is spin-coated by polymethyl methacrylate (PMMA) solution and dried

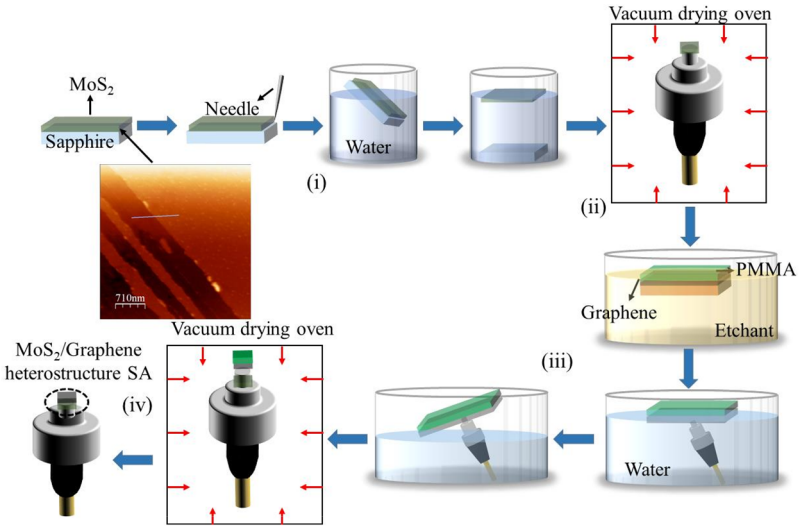

Fig. 2. Illustration of transfer process: (i) water-assisted transfer process of MoS_2 film (the inset shows its atomic force microscopic image of MoS_2 with thickness of ~3.2 nm); (ii) vacuum drying; (iii) wet transfer process of graphene film; (iv) vacuum drying; PMMA: polymethyl methacrylate.

Optical Materials EXPRESS

in air. Then we use iron nitrate solution to etch the copper. The PMMA/Graphene film is rinsed with deionized water. We place fiber connector under the film at an angle of ~30°, during which the water is drawn out with a syringe to enable the film to be attached to the substrate. From the transmittance of graphene sheet at incident white light, the graphene is estimated to be five layers. Then, we dry the sample in a vacuum drying oven to make sure the flattening of the film. Finally, acetone solution is used to remove the PMMA.

As shown in Fig. 3(a), the transmittance of heterostructure is measured from 1200 nm to 1800nm. The transmittance of sample is ~60% at 1569 nm. The interference fringe in the transmission spectrum is mainly caused by the light source. Figure 3(b) is the Raman spectrum of MoS_2/graphene heterostructure, three primary Raman peaks locating at 380.73 cm^{-1}, 402.83 cm^{-1}, and 1586 cm^{-1} are obtained by using a 532-nm laser. The Raman peaks, which are centered at 380.73 cm^{-1}, 402.83 cm^{-1}, are corresponding to E^1_{2g} and A_{1g} vibration modes, respectively, which demonstrate the structure of MoS_2 [61]. The G band at 1586 cm^{-1} confirms the presence of a graphene structure in the sample.

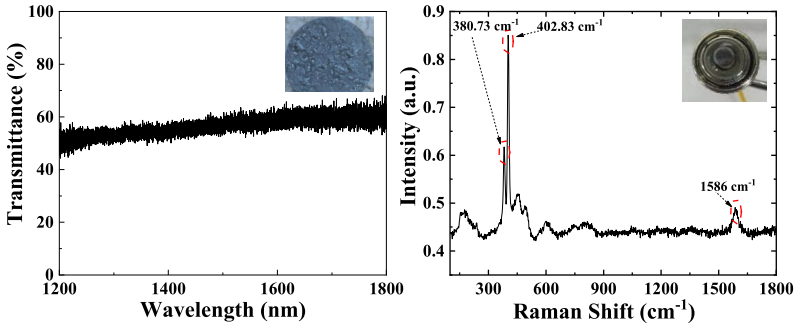

Fig. 3. (a) The measured transmittance of MoS_2/graphene heterostructure (the inset shows the microscopic image of MoS_2/graphene heterostructure integrated on fiber end); (b) the Raman spectrum of MoS_2/graphene heterostructure.

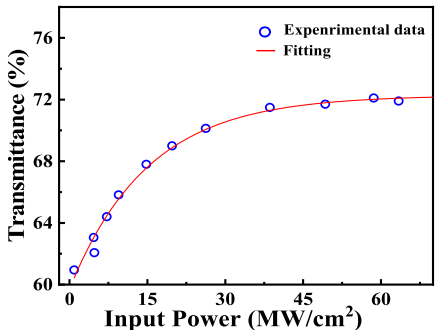

Fig. 4. The nonlinear saturable absorption of MoS_2/graphene heterostructure based SA.

We have measured the nonlinear optical response property of MoS_2/graphene heterostructure based SA. A home-made NPR-based mode-locked fiber laser operating at 1569 nm with 943-fs pulse width and 60.32-MHz repetition rate is employed as the input source. As shown in Fig. 4, according to Eq. (3), we have fitted the transmission curve. The modulation depth, the saturation intensity and the non-saturable absorbance of MoS_2/graphene heterostructure SA are 12.4%,

Optical Materials EXPRESS

12.7 MW/cm^2 and 28%, respectively. The results prove that MoS_2/graphene heterostructure can meet the essential criteria of SA for pulsed laser.

4. Experimental investigations and discussion

Figure 5 is the experimental setup of the developed mode-locked fiber laser incorporating with MoS_2/graphene heterostructure based SA. A 7.26-m-long EDF (LIEKKI 30/4) is applied as gain fiber whose second-order dispersion is + 14.2 ps^2/km at 1595 nm. The EDF is pumped by a 980-nm pump laser through wavelength-division multiplexing (WDM) coupler. The rest fiber of the laser consists of standard SMF (SMF-28) with $\beta^{(2)}_{SMF}$ at the level -22 ps^2/km and a 1.6-m-long HI1060 fiber with $\beta^{(2)}_{HI1060}$= -7 ps^2/km. A polarization-insensitive optical isolator is applied to ensure unidirectional propagation of the light in the cavity. The 90/10 coupler extracts 10% of the optical power from the laser cavity as the laser output. The mode-locking condition is optimized by the intra-cavity polarization controller (PC). The performance of the laser includes optical spectrum, pulse train, radio frequency (RF) spectrum and pulse trains are analyzed by an optical analyzer (Yokogawa AQ6375) with a spectral resolution of 0.2 nm, a real time oscilloscope (Tektronix MSO4104) with a 5-GHz photodetector, a signal source analyzer (Rohde & Schwarz, FSV30) and a commercial autocorrelator (Femtochrome, FR-103HS), respectively.

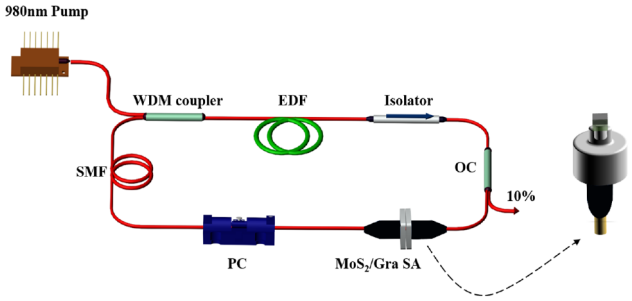

Fig. 5. Experimental setup of an erbium-doped mode-locked fiber laser. WDM coupler: wavelength-division multiplexing coupler; EDF: erbium-doped fiber; OC: output coupler; MoS_2/Gra SA: MoS_2/graphene heterostructure based saturable absorber; PC: polarization controller; SMF: single-mode fiber.

Before inserting the MoS_2/graphene heterostructure based SA into the cavity, we have investigated the operation of the fiber laser without SA to see if there is any self-mode-locking effect. No matter how we change the pump power and intra cavity polarization state, only continuous wave (CW) can be observed. Then the SA was inserted into the cavity.

In the initial state, the length of SMF is about 12.4 m, the cavity average dispersion is about -0.181 ps^2. As shown in Fig. 6(a), the Kelly sidebands in optical spectrum indicate that the fiber laser works in anomalous dispersion regime. The center wavelength is near 1596.2 nm with a 3-dB bandwidth of ~5.47 nm. The corresponding single pulse train is depicted in Fig. 6(b), showing a repetition rate of around 9.8 MHz corresponding to the cavity length. The pulse duration is also measured as shown in Fig. 6(c). The pulse width (τ_{pulse}) is calculated by multiplying the full width at half maxima of autocorrelation trace (τ_{AC}) with a coefficient. In the anomalous dispersion, the autocorrelation trace can be well fitted by hyperbolic-secant function and the pulse width is measured to be ~1.36 ps. The time-bandwidth product (TBP) is calculated to be 0.876. The slight chirp is due to the laser output after EDF with normal dispersion [17]. Figure 6(d) is the corresponding RF spectrum of the ultrashort pulses with a resolution bandwidth of 10 Hz. The two side peaks on either side of main peak in the RF spectrum indicates that the polarization

Optical Materials EXPRESS

of laser in cavity is not locked [62]. The signal-to-noise ratio (SNR) is up to ~73 dB, suggesting that the fiber laser is stable.

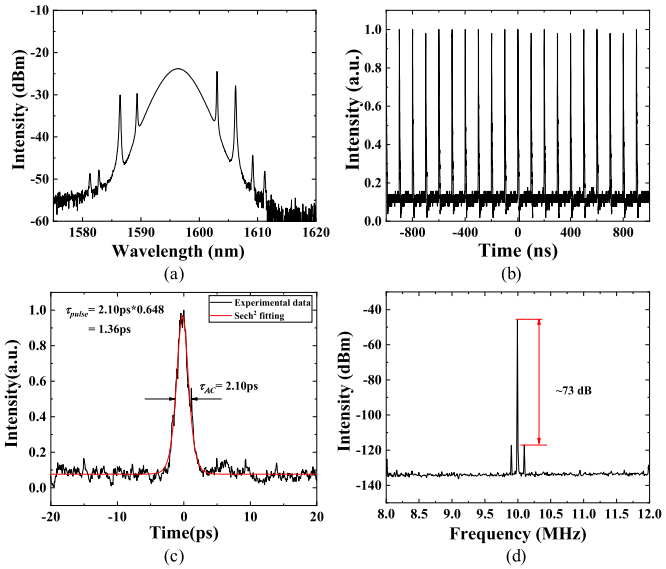

Fig. 6. The performance of laser output: (a) the optical spectrum; (b) the pulse train; (c) the autocorrelation trace; (d) the radio frequency (RF) spectrum.

In order to adjust the cavity average dispersion, we constantly cut off the single-mode fiber so that the average dispersion of the fiber laser approaches zero. Figure 7 shows how the output optical spectrum varies with different average dispersion of the dispersion-managed mode-locked fiber laser incorporating with MoS_2/graphene heterostructure based SA. At anomalous average dispersion range from -0.181 ps^2 to -0.095 ps^2, the traditional solitons have been achieved by properly adjusting PC, where the Kelly sidebands are found to superimpose on the optical spectrum. By managing the cavity average dispersion to be near zero of -0.082 ps^2, a Gaussian-like optical spectrum has been observed, which indicates that solitons have changed from traditional solitons to dispersion-managed solitons [63]. In this dispersion, the spectral bandwidth reaches its maximum which is ~11.46 nm, and the output pulse width is ~837 fs. The TBP is calculated to be 1.129. As the gain fiber plays a major role in providing the normal dispersion, the limited gain bandwidth is believed to affect the broadening of the optical spectrum. When the cavity average dispersion continues to increase to -0.071 ps^2, a small peak is observed at the center of the spectrum, the stable pulse strain cannot be obtained by adjusting the PC and pump power. Such unstable region is due to the limited gain bandwidth, and could be further minimized by a SA with larger modulation depth [15]. When the cavity average dispersion increases to normal dispersion of + 0.041 ps^2, the steep-edge optical spectrum has been produced, indicating that dissipative solitons have been generated with the bandwidth of ~10.32 nm.

Although it is difficult to estimate precisely the parameters from the real laser cavity, one can find general agreement with the numerical simulation that mode-locked fiber laser can operate from anomalous to normal average dispersion. The results have proved the successful attempt of MoS_2/graphene heterostructure based SA in dispersion-managed mode-locked fiber laser for ultrashort pulse generation from anomalous to normal average dispersion. In addition, we have tested the stability of the laser once it is mode-locked in the experiment as shown in Fig. 8. The optical spectrum of the laser output shows little change for 24 hours, indicating a stable mode-locking operation.

Optical Materials EXPRESS

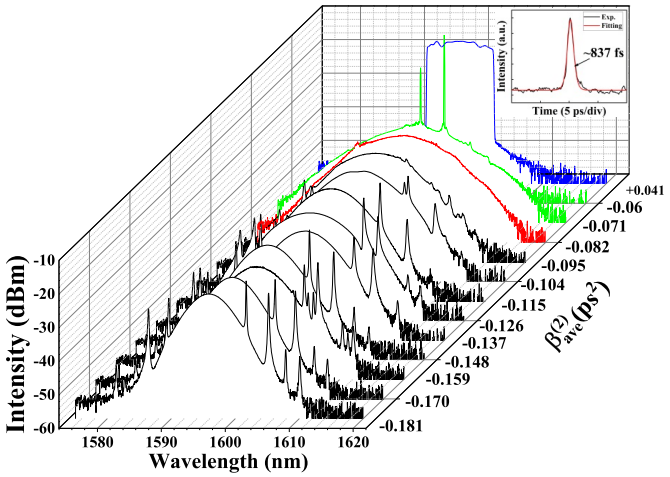

Fig. 7. The output optical spectrum of the dispersion-managed mode-locked fiber laser with different average dispersion based on MoS_2/graphene heterostructure SA (the inset shows the autocorrelation trace of ~837 fs).

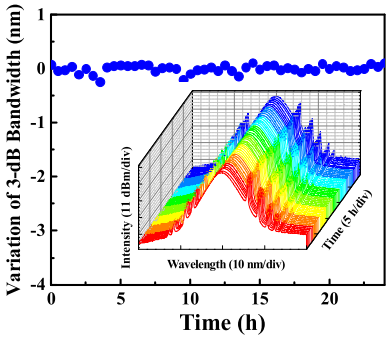

Fig. 8. The variation of 3-dB bandwidth within 24 hours (the inset shows the optical spectrum of mode-locked fiber laser incorporating MoS_2/graphene heterostructure SAs).

5. Conclusion

In conclusion, we have formed the heterostructure by transferring the MoS_2 film and graphene film to the end-facet of a fiber connector successfully. The modulation depth, the saturation intensity and the non-saturable absorption of MoS_2/graphene heterostructure are measured to be 12.4%, 12.7 MW/cm^2 and 28%, respectively. The experimental results are consistent with the results of numerical simulation. By inserting MoS_2/graphene heterostructure based SA, the erbium-doped mode-locked fiber laser can generate traditional, dispersion-management, and dissipative solitons at average anomalous, near-zero, and normal dispersion. The experimental results have validated the potential of MoS_2/graphene heterostructure as an ideal SA in dispersion-managed mode-locked fiber laser from anomalous to normal average dispersion.

Funding

National Natural Science Foundation of China (61605108, 61635006, 61735009); Shanghai Young Oriental Scholar (QD2016025); Shuguang Program (16SG35); Open Fund of the State Key Laboratory of Integrated Optoelectronics (IOSKL2019KF07).

Optical Materials EXPRESS

Acknowledgements

The authors gratefully acknowledge discussions with Q. Jiang for simulation.

Disclosures

The authors declare no conflicts of interest.

References

1. T. Yamamoto and M. Nakazawa, "Third- and fourth-order active dispersion compensation with a phase modulator in a terabit-per-second optical time-division multiplexed transmission," Opt. Lett. **26**(9), 647–649 (2001).
2. S. Wang, X. Fan, B. Wang, G. Yang, and Z. He, "Sub-THz-range linearly chirped signals characterized using linear optical sampling technique to enable sub-millimeter resolution for optical sensing applications," Opt. Express **25**(9), 10224–10233 (2017).
3. E. N. Glezer, M. Milosavljevic, L. Huang, R. J. Finlay, T. H. Her, J. P. Callan, and E. Mazur, "3-D optical storage inside transparent materials," Opt. Lett. **21**(24), 2023 (1996).
4. H. H. Liu, Y. Yu, W. Song, Q. Jiang, and F. F. Pang, "Recent development of flat supercontinuum generation in specialty optical fibers," Opto-Electronic Adv. **2**(2), 18002001–18002009 (2019).
5. K. König, O. Krauss, and I. Riemann, "Intratissue surgery with 80 MHz nanojoule femtosecond laser pulses in the near infrared," Opt. Express **10**(3), 171–176 (2002).
6. M. Sakakura, S. Kajiyama, M. Tsutsumi, J. H. Si, E. Fukusaki, Y. Tamaru, S. I. Akiyama, K. Miura, K. Hirao, and M. Ueda, "Femtosecond pulsed laser as a microscalpel for microdissection and isolation of specific sections from biological samples," Jpn. J. Appl. Phys. **46**(9A), 5859–5864 (2007).
7. Y. F. Song, J. Guo, L. M. Zhao, D. Y. Shen, and D. Y. Tang, "280 GHz dark soliton fiber laser," Opt. Lett. **39**(12), 3484–3487 (2014).
8. Y. F. Song, Z. M. Liang, H. Zhang, Q. Zhang, L. M. Zhao, D. Y. Shen, and D. Y. Tang, "Period-doubling and quadrupling bifurcation of vector soliton bunches in a graphene mode locked fiber laser," IEEE Photonics J. **9**(5), 1–8 (2017).
9. Y. F. Song, X. J. Shi, C. F. Wu, D. Y. Tang, and H. Zhang, "Recent progress of study on optical solitons in fiber lasers," Appl. Phys. Rev. **6**(2), 021313 (2019).
10. Y. F. Song, L. Li, H. Zhang, D. Y. Shen, D. Y. Tang, and K. P. Loh, "Vector multi-soliton operation and interaction in a graphene mode-locked fiber laser," Opt. Express **21**(8), 10010–10018 (2013).
11. A. M. Smirnov and O. V. Butov, "All-fiber heavily ytterbium-doped, passively mode-locked laser with the 456 MHz repetition rate," Opt. Lett. **44**(20), 5065–5068 (2019).
12. X. X. Jin, G. H. Hu, M. Zhang, Y. W. Hu, T. Albrow-Owen, R. C. T. Howe, T. C. Wu, Q. Wu, Z. Zheng, and T. Hasan, "102 fs pulse generation from a long-term stable, inkjet-printed black phosphorus-mode-locked fiber laser," Opt. Express **26**(10), 12506–12513 (2018).
13. M. Kues, C. Reimer, B. Wetzel, P. Roztocki, B. E. Little, S. T. Chu, T. Hansson, E. A. Viktorov, D. J. Moss, and R. Morandotti, "Passively mode-locked laser with an ultra-narrow spectral width," Nat. Photonics **11**(3), 159–162 (2017).
14. Y. F. Song, Z. M. Liang, X. T. Jiang, Y. X. Chen, Z. J. Li, L. Lu, Y. Q. Ge, K. Wang, J. L. Zheng, S. B. Lu, J. H. Ji, and H. Zhang, "Few-layer antimonene decorated microfiber: ultra-short pulse generation and all-optical thresholding with enhanced long term stability," 2D Mater. **4**(4), 045010 (2017).
15. H. H. Liu and K. K. Chow, "Enhanced stability of dispersion-managed mode-locked fiber lasers with near-zero net cavity dispersion by high-contrast saturable absorbers," Opt. Lett. **39**(1), 150–153 (2014).
16. N. Nishizawa, Y. Nozaki, E. Itoga, H. Kataura, and Y. Sakakibara, "Dispersion-managed, high-power, Er-doped ultrashort-pulse fiber laser using carbon-nanotube polyimide film," Opt. Express **19**(22), 21874–21879 (2011).
17. X. M. Liu, "Soliton formation and evolution in passively-mode-locked lasers with ultralong anomalous-dispersion fibers," Phys. Rev. A **84**(2), 023835 (2011).
18. S. Chouli, J. M. Soto-Crespo, and P. Grelu, "Optical spectra beyond the amplifier bandwidth limitation in dispersion-managed mode-locked fiber lasers," Opt. Express **19**(4), 2959–2964 (2011).
19. P. Grelu and N. Akhmediev, "Dissipative solitons for mode-locked lasers," Nat. Photonics **6**(2), 84–92 (2012).
20. X. M. Liu, "Dynamic evolution of temporal dissipative-soliton molecules in large normal path-averaged dispersion fiber lasers," Phys. Rev. A **82**(6), 063834 (2010).
21. Y. Z. Wang, L. Q. Zhang, Z. Zhuo, and S. Z. Guo, "Cross-splicing method for compensating fiber birefringence in polarization-maintaining fiber ring laser mode locked by nonlinear polarization evolution," Appl. Opt. **55**(21), 5766–5770 (2016).
22. Z. P. Sun, D. Popa, T. Hasan, F. Torrisi, F. Q. Wang, E. J. R. Kelleher, J. C. Travers, V. Nicolosi, and A. C. Ferrari, "A stable, wideband tunable, near transform-limited, graphene-mode-locked, ultrafast laser," Nano Res. **3**(9), 653–660 (2010).
23. Z. Luo, M. Zhou, J. Weng, G. Huang, H. Xu, C. Ye, and Z. Cai, "Graphene-based passively Q-switched dual-wavelength erbium-doped fiber laser," Opt. Lett. **35**(21), 3709–3711 (2010).

Optical Materials EXPRESS

24. Q. L. Bao, H. Zhang, Y. Wang, Z. H. Ni, Y. L. Yan, Z. X. Shen, K. P. Loh, and D. Y. Tang, "Atomic-layer graphene as a saturable absorber for ultrafast pulsed lasers," Adv. Funct. Mater. **19**(19), 3077–3083 (2009).
25. Y. F. Song, H. Zhang, D. Y. Tang, and D. Y. Shen, "Polarization rotation vector solitons in a graphene mode-locked fiber laser," Opt. Express **20**(24), 27283–27289 (2012).
26. X. H. Li, Y. G. Wang, Y. S. Wang, Y. Z. Zhang, K. Wu, P. P. Shum, X. Yu, Y. Zhang, and Q. J. Wang, "All-normal-dispersion passively mode-locked Yb-doped fiber ring laser based on a graphene oxide saturable absorber," Laser Phys. Lett. **10**(7), 075108 (2013).
27. M. Zhang, Q. Wu, F. Zhang, L. L. Chen, X. X. Jin, Y. W. Hu, Z. Zheng, and H. Zhang, "2D black phosphorus saturable absorbers for ultrafast photonics," Adv. Opt. Mater. **7**(1), 1800224 (2019).
28. Z. N. Guo, H. Zhang, S. B. Lu, Z. T. Wang, S. Y. Tang, J. D. Shao, Z. B. Sun, H. H. Xie, H. Y. Wang, X. F. Yu, and P. K. Chu, "From black phosphorus to phosphorene: basic solvent exfoliation, evolution of Raman scattering, and applications to ultrafast photonics," Adv. Funct. Mater. **25**(45), 6996–7002 (2015).
29. Y. H. Xu, Z. T. Wang, Z. N. Guo, H. Huang, Q. L. Xiao, H. Zhang, and X. F. Yu, "Solvothermal synthesis and ultrafast photonics of black phosphorus quantum dots," Adv. Opt. Mater. **4**(8), 1223–1229 (2016).
30. Z. Luo, D. Wu, B. Xu, H. Xu, Z. Cai, J. Peng, J. Weng, S. Xu, C. Zhu, F. Wang, Z. Sun, and H. Zhang, "Two-dimensional material-based saturable absorbers: Towards compact visible-wavelength all-fiber pulsed lasers," Nanoscale **8**(2), 1066–1072 (2016).
31. K. Wu, X. Y. Zhang, J. Wang, X. Li, and J. P. Chen, "WS2 as a saturable absorber for ultrafast photonic applications of mode-locked and Q-switched lasers," Opt. Express **23**(9), 11453–11461 (2015).
32. K. Wu, X. Y. Zhang, J. Wang, and J. P. Chen, "463-MHz fundamental mode-locked fiber laser based on few-layer MoS2 saturable absorber," Opt. Lett. **40**(7), 1374–1377 (2015).
33. H. Zhang, S. B. Lu, J. Zheng, J. Du, S. C. Wen, D. Y. Tang, and K. P. Loh, "Molybdenum disulfide (MoS_2) as a broadband saturable absorber for ultra-fast photonics," Opt. Express **22**(6), 7249–7260 (2014).
34. H. Long, S. X. Liu, Q. Wen, H. Y. Yuan, C. Y. Tang, J. L. Qu, S. N. Ma, W. Qarony, L. H. Zeng, and Y. H. Tsang, "In2Se3 nanosheets with broadband saturable absorption used for near-infrared femtosecond laser mode locking," Nanotechnology **30**(46), 465704 (2019).
35. T. Chai, X. H. Li, T. C. Feng, P. L. Guo, Y. F. Song, Y. X. Chen, and H. Zhang, "Few-layer bismuthene for ultrashort pulse generation in a dissipative system based on an evanescent field," Nanoscale **10**(37), 17617–17622 (2018).
36. Z. J. Xie, C. Y. Xing, W. C. Huang, T. J. Fan, Z. J. Li, J. L. Zhao, Y. J. Xiang, Z. N. Guo, J. Q. Li, Z. G. Yang, B. Q. Dong, J. L. Qu, D. Y. Fan, and H. Zhang, "Ultrathin 2D nonlayered tellurium nanosheets: facile liquid-phase exfoliation, characterization, and photoresponse with high performance and enhanced stability," Adv. Funct. Mater. **28**(16), 1705833 (2018).
37. C. Y. Xing, Z. J. Xie, Z. M. Liang, W. Y. Liang, T. J. Fan, J. S. Ponraj, S. C. Dhanabalan, D. Y. Fan, and H. Zhang, "2D nonlayered selenium nanosheets: facile synthesis, photoluminescence, and ultrafast photonics," Adv. Opt. Mater. **5**(24), 1700884 (2017).
38. L. M. Wu, Z. J. Xie, L. Lu, J. L. Zhao, Y. Z. Wang, X. T. Jiang, Y. Q. Ge, F. Zhang, S. B. Lu, Z. N. Guo, J. Liu, Y. J. Xiang, S. X. Xu, J. Q. Li, D. Y. Fan, and H. Zhang, "Few-layer tin sulfide: a promising black-phosphorus-analogue 2D material with exceptionally large nonlinear optical response, high stability, and applications in all-optical switching and wavelength conversion," Adv. Opt. Mater. **6**(2), 1700985 (2018).
39. Z. J. Xie, F. Zhang, Z. M. Liang, T. J. Fan, Z. J. Li, X. T. Jiang, H. Chen, J. Q. Li, and H. Zhang, "Revealing of the ultrafast third-order nonlinear optical response and enabled photonic application in two-dimensional tin sulfide," Photonics Res. **7**(5), 494–502 (2019).
40. Y. P. Zhang, C. K. Lim, Z. G. Dai, G. N. Yu, J. W. Haus, H. Zhang, and P. N. Prasad, "Photonics and optoelectronics using nano-structured hybrid perovskite media and their optical cavities," Phys. Rep. **795**, 1–51 (2019).
41. P. F. Li, Y. Chen, T. S. Yang, Z. Y. Wang, H. Lin, Y. H. Xu, L. Li, H. R. Mu, B. N. Shivananju, Y. P. Zhang, Q. L. Zhang, A. L. Pan, S. J. Li, D. Y. Tang, B. H. Jia, H. Zhang, and Q. L. Bao, "Two-dimensional CH3NH3PbI3 perovskite nanosheets for ultrafast pulsed fiber lasers," ACS Appl. Mater. Interfaces **9**(14), 12759–12765 (2017).
42. X. T. Jiang, W. J. Li, T. Hai, R. Yue, Z. W. Chen, C. S. Lao, Y. Q. Ge, G. Q. Xie, Q. Wen, and H. Zhang, "Inkjet-printed MXene micro-scale devices for integrated broadband ultrafast photonics," npj 2D Mater. Appl. **3**(1), 9 (2019).
43. X. T. Jiang, H. L. Lu, Q. Li, H. Zhou, S. D. Zhang, and H. Zhang, "Epsilon-near-zero medium for optical switches in a monolithic waveguide chip at 1.9 mu m," Nanophotonics **7**(11), 1835–1843 (2018).
44. X. T. Jiang, S. Gross, M. J. Withford, H. Zhang, D. I. Yeom, F. Rotermund, and A. Fuerbach, "Low-dimensional nanomaterial saturable absorbers for ultrashort-pulsed waveguide lasers," Opt. Mater. Express **8**(10), 3055–3071 (2018).
45. M. J. Allen, V. C. Tung, and R. B. Kaner, "Honeycomb carbon: a review of graphene," Chem. Rev. **110**(1), 132–145 (2010).
46. R. R. Nair, P. Blake, A. N. Grigorenko, K. S. Novoselov, T. J. Booth, T. Stauber, N. M. R. Peres, and A. K. Geim, "Fine structure constant defines visual transparency of graphene," Science **320**(5881), 1308 (2008).
47. S. X. Wang, H. H. Yu, H. J. Zhang, A. Z. Wang, M. W. Zhao, Y. X. Chen, L. M. Mei, and J. Y. Wang, "Broadband few-layer MoS_2 saturable absorbers," Adv. Mater. **26**(21), 3538–3544 (2014).
48. G. Zhao, J. Hou, Y. Z. Wu, J. L. He, and X. P. Hao, "Preparation of 2D MoS_2/Graphene heterostructure through a monolayer intercalation method and its application as an optical modulator in pulsed laser generation," Adv. Opt. Mater. **3**(7), 937–942 (2015).

Optical Materials EXPRESS

49. O. Lopez-Sanchez, E. Alarcon Llado, V. Koman, A. F. I. Morral, A. Radenovic, and A. Kis, "Light generation and harvesting in a van der Waals heterostructure," ACS Nano **8**(3), 3042–3048 (2014).
50. A. Azizi, S. Eichfeld, G. Geschwind, K. H. Zhang, B. Jiang, D. Mukherjee, L. Hossain, A. F. Piasecki, B. Kabius, J. A. Robinson, and N. Alem, "Freestanding van der Waals heterostructures of graphene and transition metal dichalcogenides," ACS Nano **9**(5), 4882–4890 (2015).
51. Z. Y. Huang, W. J. Han, H. L. Tang, L. Ren, D. S. Chander, X. Qi, and H. Zhang, "Photoelectrochemical-type sunlight photodetector based on MoS2/graphene heterostructure," 2D Mater. **2**(3), 035011 (2015).
52. C. H. Lee, G. H. Lee, A. M. van der Zande, W. C. Chen, Y. L. Li, M. Y. Han, X. Cui, G. Arefe, C. Nuckolls, T. F. Heinz, J. Guo, J. Hone, and P. Kim, "Atomically thin p-n junctions with van der Waals heterointerfaces," Nat. Nanotechnol. **9**(9), 676–681 (2014).
53. K. Chang and W. X. Chen, "L-Cysteine-assisted synthesis of layered MoS_2/Graphene composites with excellent electrochemical performances for lithium ion batteries," ACS Nano **5**(6), 4720–4728 (2011).
54. Y. J. Gong, S. B. Yang, Z. Liu, L. L. Ma, R. Vajtai, and P. M. Ajayan, "Graphene-network-backboned architectures for high-performance lithium storage," Adv. Mater. **25**(29), 3979–3984 (2013).
55. Y. Q. Jiang, L. L. Miao, G. B. Jiang, Y. Chen, X. Qi, X. F. Jiang, H. Zhang, and S. C. Wen, "Broadband and enhanced nonlinear optical response of MoS_2/graphene nanocomposites for ultrafast photonics applications," Sci. Rep. **5**(1), 16372 (2015).
56. M. M. He, C. J. Quan, C. He, Y. Y. Huang, L. P. Zhu, Z. H. Yao, S. J. Zhang, J. T. Bai, and X. L. Xu, "Enhanced nonlinear saturable absorption of MoS_2/graphene nanocomposite films," J. Phys. Chem. C **121**(48), 27147–27153 (2017).
57. G. P. Agrawal, *Nonlinear fiber optics* (Springer, 2000).
58. Y. Zhang, J. Q. Zhu, P. X. Li, X. X. Wang, H. Yu, K. Xiao, C. Y. Li, and G. Y. Zhang, "All-fiber Yb-doped fiber laser passively mode-locking by monolayer MoS_2 saturable absorber," Opt. Commun. **413**, 236–241 (2018).
59. A. Gurarslan, Y. F. Yu, L. Q. Su, Y. L. Yu, F. Suarez, S. S. Yao, Y. Zhu, M. Ozturk, Y. Zhang, and L. Y. Cao, "Surface-energy-assisted perfect transfer of centimeter-scale monolayer and few-layer MoS_2 films onto arbitrary substrates," ACS Nano **8**(11), 11522–11528 (2014).
60. J. W. Suk, A. Kitt, C. W. Magnuson, Y. F. Hao, S. Ahmed, J. H. An, A. K. Swan, B. B. Goldberg, and R. S. Ruoff, "Transfer of CVD-grown monolayer graphene onto arbitrary substrates," ACS Nano **5**(9), 6916–6924 (2011).
61. H. Li, Q. Zhang, C. C. R. Yap, B. K. Tay, T. H. T. Edwin, A. Olivier, and D. Baillargeat, "From bulk to monolayer MoS_2: evolution of Raman scattering," Adv. Funct. Mater. **22**(7), 1385–1390 (2012).
62. S. T. Cundiff, B. C. Collings, and W. H. Knox, "Polarization locking in an isotropic, mode locked soliton Er/Yb fiber laser," Opt. Express **1**(1), 12–20 (1997).
63. H. A. Haus, K. Tamura, L. E. Nelson, and E. P. Ippen, "Stretched-pulse additive pulse mode-locking in fiber ring lasers: theory and experiment," IEEE J. Quantum Electron. **31**(3), 591–598 (1995).